Resource-Efficient Quantum Beneš Networks

Shu-Ming Hu(胡书鸣)[1,2], Jun-Hao Wei(魏君豪)[1,2], Nuo-Ya Yang(杨挪亚)[1,2], Li Li(李力)[1,2,3*], Nai-Le Liu(刘乃乐)[1,2,3*], and Kai Chen(陈凯)[1,2,3*]

[1]*Hefei National Research Center for Physical Sciences at the Microscale and School of Physical Sciences, University of Science and Technology of China, Hefei 230026, China*
[2]*CAS Center for Excellence in Quantum Information and Quantum Physics, University of Science and Technology of China, Hefei 230026, China*
[3]*Hefei National Laboratory, University of Science and Technology of China, Hefei 230088, China*

Distributing quantum states and entanglement between multiple pairs of nodes is a fundamental task in quantum communication and distributed quantum computing on large-scale quantum networks. In particular, the simultaneous distribution of quantum states or entanglement among multiple source-destination pairs (quantum k-pair communication task) is an emerging demand for scalable quantum networks. Here, we propose a quantum network architecture based on the Beneš switching topology that provides a universal switching framework for such pairwise communications. Our network architecture requires only $\mathcal{O}(k \log k)$ pre-established entangled resources to accomplish the k-pair communication task, and offers advantages of non-blocking and low latency. We develop routing protocols for concurrent entanglement distribution and analyze their performance under ideal operating assumptions, while also discussing the effects of nonideal entanglement generation, quantum memory decoherence, photon loss, and finite Bell state measurement (BSM) success probability. The proposed framework requires local BSMs and entanglement swapping operations and is compatible in principle with quantum platforms supporting these capabilities. In particular, photonic implementations can benefit from mature photonic components and be compatible with existing telecommunications infrastructure.

Keywords: quantum Beneš network, quantum network routing, entanglement distribution

PACS: 03.67.Hk, 03.67.Ac

1.Introduction. Quantum networks are envisioned as a foundational infrastructure for the emerging quantum internet, with recent roadmap studies identifying key milestones and architectural requirements for scalable quantum networking [1–3], enabling the distribution of quantum states and entanglement across spatially separated nodes to support quantum communication, distributed quantum computing, and secure cryptography [4–11]. By interconnecting remote quantum devices through photonic or hybrid interfaces, such networks allow distant parties to share entangled resources, perform quantum teleportation, and implement nonlocal operations that surpass the capabilities of isolated systems [1,4,12–16].

Recent experimental advances have realized many of these fundamental building blocks, including metropolitan-scale fiber networks for entanglement distribution, satellite-based free-space quantum links spanning thousands of kilometers, and elementary quantum repeater nodes capable of entanglement swapping and quantum state storage [13,17–24]. More recent progress includes entanglement distribution over deployed optical fibers, the coexistence of quantum teleportation with classical communications, and advances in long-distance quantum key distribution and quantum-network routing [25–30]. Furthermore, high-fidelity entanglement generation over extended distances has been demonstrated across multiple platforms [31–37]. Photonic systems offer intrinsic advantages for long-distance entanglement distribution: photons interact weakly with their environment during propagation, are compatible with existing telecommunications infrastructure, and benefit from mature photonic component technologies [35,36,38,39]. These advances indicate the feasibility of large-scale quantum interconnects and pave the way toward increasingly complex networked quantum systems composed of numerous communicating users and quantum processors.

As quantum networks scale to larger numbers of nodes and users, the efficient distribution of quantum states and entanglement becomes increasingly critical. Long-distance quantum communication typically relies on entanglement-based primitives such as quantum teleportation, which enables the faithful transfer of unknown quantum states, and quantum repeaters, which extend communication distances through entanglement swapping and quantum memories [4,14,40,41]. However, the generation, storage, and transmission of high-fidelity entanglement remain resource intensive and highly susceptible to photon loss, decoherence, and operational noise, particularly in large-scale quantum networks [42,43]. These physical limitations make entanglement distribution inherently probabilistic and costly, requiring repeated attempts and substantial coordination across the network. The challenge is further exacerbated when multiple pairs of nodes simultaneously request quantum communication or shared entanglement, as competing demands for limited channels and intermediate nodes can lead to congestion and conflicts, thereby substantially reducing overall throughput, highlighting the importance of efficient entanglement routing strategies in large-scale quantum networks [44–46]. These considerations highlight the need for scalable routing and switching strategies that can systematically coordinate numerous concurrent quantum connections, motivating structured approaches such as quantum network coding (QNC) and

*Corresponding authors. Email: eidos@ustc.edu.cn; nlliu@ustc.edu.cn; kaichen@ustc.edu.cn

permutation based switching architectures [47–52].

In classical communication networks, network coding provides a powerful solution for improving throughput and resolving contention by allowing intermediate nodes to process and combine information flows rather than merely forwarding them [53]. Inspired by this concept, QNC has been proposed to enhance the efficiency of entanglement and quantum state distribution in multi-user quantum networks [47,48]. Early approaches rely on pre-shared entanglement and classical side communication to simulate coding operations [49], whereas subsequent schemes incorporate repeater-assisted protocols that exploit local processing at intermediate nodes [50,54]. More recently, measurement-based and cluster-state-based constructions have been developed to realize coding functionalities through adaptive measurements and feedforward operations [51,55,56]. Despite these advances, existing QNC and MQNC protocols are generally tailored to prescribed network topologies and communication tasks, and their resource states and measurement patterns may depend on the specific network under consideration. In particular, mappings based on linear network codes can require the generation of two-colorable graph states at individual nodes, and embedding such resources into a given network structure in which each node holds a single qubit is not straightforward [45]. These topology- and resource-dependent requirements make their direct extension to universal k-pair permutation switching nontrivial, motivating a complementary architecture-based approach using rearrangeable or non-blocking switching networks [57,58].

Classical switching networks offer a complementary approach to contention that relies not on coding but on carefully designed interconnection architectures that realize deterministic and conflict-free routing [57–60]. Instead of combining information flows, switching networks physically rearrange connections between inputs and outputs to implement prescribed communication patterns. Among these architectures, rearrangeable and non-blocking networks play a central role, as they guarantee that any set of source-destination pairings, or equivalently any permutation, can be established without interference. A particularly attractive example is the Beneš network [61–63], which achieves universal permutation routing using a fixed multistage structure with logarithmic depth and near-optimal hardware complexity. Its regular topology, scalability, and reconfigurability make it well suited for large-scale systems requiring efficient support for dynamic and parallel connections. These features suggest that classical switching architectures, and the Beneš network in particular, provide a natural blueprint for designing scalable quantum routing mechanisms.

In this work, we develop a quantum switching architecture based on the Beneš topology. Our construction realizes a fixed-structure quantum network that supports arbitrary k-pair routing tasks through a unified routing protocol, using only $O(k \log k)$ shared entangled pairs across the network. This architecture therefore provides a resource-efficient and universal switching framework for large-scale quantum networks, significantly reducing the entanglement resources required for flexible multi-pair communication. The protocol configures the network via local operations and classical coordination to establish the required end-to-end quantum connections while keeping the underlying hardware topology unchanged. Importantly, the proposed architecture is largely implementation-agnostic: it requires only standard capabilities at each node, namely BSMs and entanglement swapping, and can in principle be implemented across different physical platforms supporting these operations. Furthermore, by exploiting parallel operations and techniques inspired by quantum wireless multihop networks [64], where simultaneous measurements replace sequential entanglement swapping, our scheme enables low-latency entanglement distribution and offers significant practical advantages for scalable quantum networking. Taken together, these features provide a scalable and resource-efficient framework for rearrangeably non-blocking permutation routing in large-scale quantum networks.

2.Background. Efficient transmission of quantum information among multiple users is a fundamental task in large-scale quantum networks. While quantum teleportation and entanglement swapping enable long-distance communication [14,65], simultaneous transmissions may create bottlenecks due to limited network resources. To address this challenge, two representative approaches have been investigated. QNC, inspired by classical network coding [53], improves communication efficiency through quantum operations, measurements, and classical communication [47–51,54,55]. Alternatively, switching-network architectures provide deterministic routing with low structural complexity and have been widely adopted in classical communication systems [57,59]. In the following, we briefly review representative QNC protocols and the classical Beneš network, which forms the basis of the proposed quantum Beneš network.

2.1.The quantum network coding. The butterfly network serves as the canonical benchmark for studying quantum network coding, as it represents the simplest communication scenario exhibiting a network bottleneck. In classical networks, the intermediate node resolves the bottleneck by performing a coding operation. However, this strategy cannot be directly extended to the quantum two-pair problem because the no-cloning theorem forbids copying unknown quantum states. Hayashi *et al.* first investigated this problem and proved that perfect quantum state transmission over the butterfly network is impossible without additional resources [48,49]. They further showed that perfect QNC becomes achievable when prior entanglement is shared between the two senders, where quantum teleportation together with classical network coding enables successful cross transmission [49]. This protocol was later experimentally demonstrated by He Lu *et al.* in a photonic platform [44]. Subsequent studies extended the butterfly-network framework to the general k-pair problem, QNC with free classical communication, and nonlinear QNC protocols, among other advances [66–70].

To support long-distance quantum communication over quantum networks with complex topologies, Satoh *et al.* developed QNC for general quantum repeater networks [50,54]. In these networks, adjacent repeater nodes initially share a single Einstein–Podolsky–Rosen (EPR) pair but cannot introduce additional quantum registers or directly transmit quantum information, as illustrated in Fig. 1. The protocol manipulates these EPR pairs using two basic operations termed “Connection” and “Removal.” The Connection operation uses an EPR pair shared between adjacent nodes

to extend the entanglement correlation of a local qubit to the neighboring node through local gates, measurement, and classical feed-forward. The Removal operation eliminates an intermediate resource qubit through measurement and conditional correction while preserving the required correlations among the remaining qubits. By combining these operations, QNC transforms the initially shared link-level EPR pairs into the desired end-to-end Bell pairs for specific network topologies.

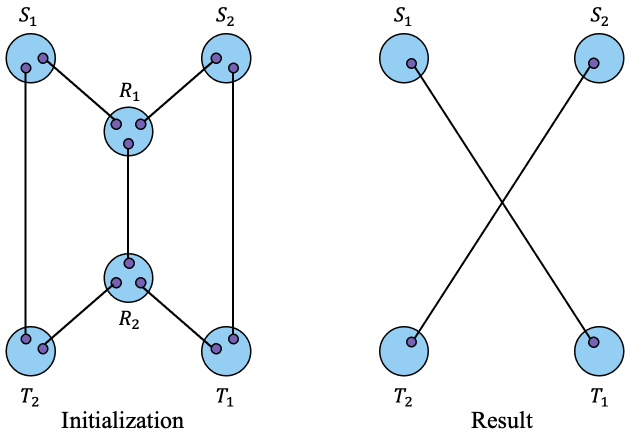


Figure 1: Initial entanglement resources and final states of QNC based on quantum repeaters. The blue circles represent quantum repeater nodes, the purple dots represent their local quantum memory qubits, and the lines connecting the memory qubits represent shared EPR pairs. S_1 and S_2 are the sender nodes, T_1 and T_2 are the target nodes, and R_1 and R_2 are the intermediate resource nodes. The goal is to transform the initial link-level EPR pairs into Bell pairs shared between S_1 and T_1 and between S_2 and T_2 through a sequence of Connection and Removal operations described in the main text.

Inspired by one-way quantum computation, measurement-based quantum network coding (MQNC) provides a measurement-based alternative to the repeater network protocol with reduced circuit depth [51,55,71]. The MQNC protocols employ cluster states as the resource states, which can be generated from multiple shared EPR pairs. By measuring the two central qubits in the X basis, cross entanglement can be established in the network, whereas straight entanglement can be realized by measuring the same qubits in the Z basis, as shown in Fig. 2. Several studies have further investigated the QNC based on quantum repeaters and MQNC frameworks, such as general QNC protocol for large-scale quantum networks, analyses of QNC and MQNC protocols over repeater networks under noisy conditions, modeling of MQNC on superconducting quantum processors, and so on [54,55,68,71].

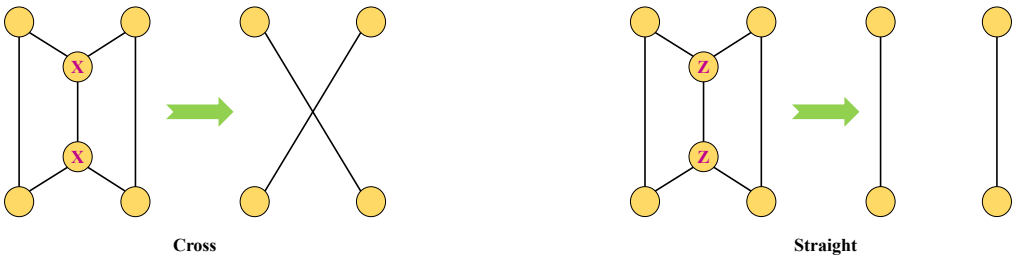


Figure 2: The procedure for MQNC with a six-qubit cluster state. Circles and lines represent qubits and entanglement between qubits. The cross pairs can be established by measuring the two central qubits in the X basis, while the straight pairs can be established by measuring the two central qubits in the Z basis.

Overall, existing QNC protocols have demonstrated the effectiveness of coding-based strategies for alleviating communication bottlenecks in quantum networks. However, these protocols are typically tailored to specific network topologies, and extending them to large-scale communication networks often requires increasingly complicated protocol designs. As a result, current QNC schemes lack a unified and systematic network architecture that naturally supports scalability. This motivates us to look beyond individual coding protocols and investigate well-established network architectures

developed in classical communication systems. Among them, the Beneš network is particularly attractive because of its regular topology, recursive construction, and rearrangeably non-blocking property.

2.2.The Beneš switching network. To address the scalability limitations of existing QNC protocols, it is natural to seek a network architecture that supports systematic construction while preserving efficient communication. Classical multistage switching networks provide such a framework, among which the Beneš network is one of the most representative architectures [61,72]. The Beneš network realizes arbitrary input-output permutations using a fixed interconnection structure and is rearrangeably non-blocking, meaning that any communication pattern can always be established through appropriate switch configurations. Owing to its recursive construction, regular topology, and logarithmic network depth, it has been widely adopted in communication systems, parallel interconnects, and switching fabrics for scalable permutation routing [62,63]. Figure 3(a) illustrates a classical 4×4 Beneš switching network with four input ports, four output ports, and three stages of 2×2 switching elements. The two configurations of an elementary switching element are shown in Fig. 3(b).

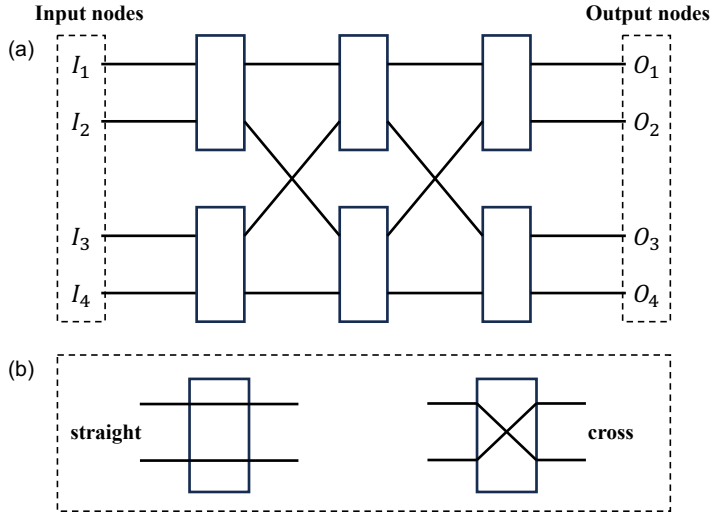


Figure 3: Structure and switching modes of a classical 4×4 Beneš network. (a) The network consists of three stages, each containing two 2×2 switching elements. (b) The straight and cross configurations of a 2×2 switching element. In the straight configuration, each input is connected to the corresponding output, whereas in the cross configuration, the two connections are interchanged.

Structurally, a Beneš network of size $k = 2^n$ is constructed recursively from two Beneš subnetworks of size $k/2$, together with an initial and a final stage of 2×2 switching elements. The resulting network contains $2\log_2 k - 1$ stages, each consisting of $k/2$ elementary 2×2 switching elements. Each element can be independently configured in either the straight or cross state, thereby determining the paths through the network. For any desired input-output permutation, a routing algorithm assigns an appropriate state to every switching element so that all inputs are connected to their respective target outputs without conflict. This recursive structure makes the Beneš network rearrangeably non-blocking: any input-output permutation can be realized within the fixed topology by reconfiguring its local switching elements.

Compared with other classical switching architectures, the Beneš switching network offers notable advantages in terms of resource overhead and congestion. A full crossbar switch network requires $\mathcal{O}(k^2)$ hardware resources [59], which quickly becomes impractical for large systems. Butterfly and Clos networks reduce hardware cost but may suffer from blocking [57,59]. In contrast, the Beneš network achieves rearrangeable non-blocking operation using only $\mathcal{O}(k \log k)$ switching elements and logarithmic depth, thereby providing both scalability and low latency. Moreover, its fixed, regular, and recursive structure simplifies control and implementation while guaranteeing universal permutation capability. These properties position the Beneš architecture as a natural candidate for constructing scalable, non-blocking, and low-latency quantum switching networks [73,74].

3.Quantum Beneš network. Based on the classical Beneš switching network, we develop a scalable quantum network architecture together with its routing protocol. Instead of designing a routing strategy for a specific communication scenario, the proposed framework provides a systematic construction for arbitrary network sizes while preserving the non-blocking property of the Beneš architecture. The network architecture, routing protocol, and a representative 4×4 example are presented in the following.

3.1.Network architecture. We begin by introducing the quantum Beneš network architecture designed to support arbitrary k-pair communication tasks. Our construction extends the classical Beneš switching topology to the quantum

domain by replacing classical switching operations with entangled states, local operations, and measurements. Unlike physical nearest-neighbor lattice models, the proposed architecture follows the logical connectivity of a general Beneš network, where entanglement links may be established between nodes that are not necessarily adjacent in physical space. This abstraction allows us to focus on the routing and switching functionality of the network independently of a specific hardware layout while retaining the structural advantages of the Beneš topology.

For clarity, we first introduce the quantum Beneš network for sizes that are powers of 2. The construction can be extended recursively to an arbitrary size k by using an upper subnetwork of size $\lfloor k/2 \rfloor$ and a lower subnetwork of size $\lceil k/2 \rceil$. When k is even, the two subnetworks have the same size. When k is odd, the last input and output nodes are connected exclusively to the larger lower subnetwork, whereas the remaining nodes are connected to both subnetworks through the input and output switching layers. Recursively applying this decomposition until subnetworks of size 1 or 2 are reached yields a quantum Beneš network for any positive integer k, while retaining an $\mathcal{O}(k \log k)$ resource overhead. Further details are provided in the Supplementary Material.

In a classical Beneš switching network, switches are interconnected via classical communication channels. In contrast, in our quantum Beneš architecture, the connections between switching elements are realized through quantum teleportation. Each node is required to be capable of performing quantum operations, BSMs, and classical communication. Unlike Spanke-Beneš or nearest-neighbor architectures [72], we do not require that only physically adjacent nodes share entanglement. Instead, any pair of nodes connected in the Beneš topology is assumed to be able to pre-establish Bell pairs through underlying physical mechanisms such as photonic transmission, quantum repeaters, or entanglement distribution protocols. These entangled links serve as the fundamental resources for subsequent entanglement swapping and quantum state teleportation.

The routing protocol developed in this work is formulated at the switching layer and assumes ideal operation: the Bell pairs required by the selected routes are assumed to have been successfully established before the corresponding BSMs are performed. Their physical generation is treated as an underlying link-layer service, allowing us to focus on how the available entangled links are selected and measured to realize an arbitrary input-output permutation.

Quantum memories are local components of the repeater nodes rather than separate network nodes. They store the local halves of successfully generated Bell pairs until a valid routing configuration is identified and the corresponding BSMs are performed. A destination memory may additionally retain the resulting qubit until the measurement outcomes are received and the required local correction is applied. Because each incident entanglement link requires one memory qubit to store its local half, an internal repeater connected to two nodes in each adjacent layer requires at least four memory qubits to hold all candidate link resources. Additional memories may be needed for multiplexed entanglement generation, purification, or multiple candidate Bell pairs, but these resources are not included in the minimal architectural model considered here.

A $2k$-port quantum Beneš network can be constructed recursively from two k-port quantum Beneš subnetworks. Then, the quantum Beneš network can be conceptually divided into three layers. The two k-port subnetworks form the switching layer; the nodes connected to both the input ports and the subnetworks constitute the input layer; and the nodes connected to both the output ports and the subnetworks constitute the output layer. In general, for a $2k$-port quantum Beneš network, the ith node in the input or output layer shares entangled states with the $(i+k)$th (or $(i-k)$th) node in the switching layer when $i \leq k$ (or $i > k$), respectively.

The fundamental building block of the quantum Beneš network is a 2×2 quantum switching module, which serves as the quantum analogue of a classical switching element. In a classical Beneš network, each switching element can be configured into either a straight or a cross state, thereby routing incoming signals to appropriate output ports. The 2×2 quantum switching module can be realized using entangled states, local operations and measurements. One direct approach is to establish entangled states between each input node and each output node. The switching functionality is implemented via entanglement swapping. The connection between the desired input-output node pair can then be established by performing BSMs on the appropriate qubits. Here, we label the entangled states shared between the first (second) input node and the first (second) output node as straight states, the entangled states shared between the first (second) input node and the second (first) output node as cross states. To realize the straight mode, the switching nodes perform BSMs on the qubits corresponding to straight states. To realize the cross mode, the switching nodes perform BSMs on the qubits corresponding to cross states.

For a near-term photonic implementation of the proposed quantum Beneš network, direct entanglement swapping based on pairwise Bell states is the most practical of the three considered approaches. Because the Beneš topology resolves blocking through its switching structure, network coding is not required under the present architectural assumptions. The direct scheme uses only bipartite Bell states and BSMs, avoiding the preparation and control of multipartite resource states. Although photon loss and finite detector efficiency reduce the success probabilities of Bell-pair generation and BSMs, its comparatively simple requirements for resource preparation, synchronization, and detection make it more suitable for current photonic platforms. QNC and MQNC remain useful alternatives when the available physical topology is fixed and contains unavoidable bottlenecks [50,55]. Compared with repeater-based QNC, MQNC reduces the circuit depth by encoding the required operations into a multipartite graph or cluster state, but preparing and detecting such states places greater demands on photon generation, synchronization, and detection. We therefore use direct entanglement swapping as the reference implementation, while QNC and MQNC may be considered for topology-constrained scenarios in which network coding provides an advantage.

3.2.Routing protocol. Having established the structure of the quantum Beneš network and the operation of the 2×2 quantum switching module, we now describe the routing protocol that enables arbitrary k-pair quantum communication. The protocol specifies how entanglement swapping and teleportation operations are scheduled to realize a given source-destination permutation. We consider a set of k source nodes $\{S_1, \ldots, S_k\}$ and k destination nodes $\{D_1, \ldots, D_k\}$, where each source node S_i aims to establish either an end-to-end entangled pair with $D_{\pi(i)}$ or to teleport an unknown quantum state to $D_{\pi(i)}$ for some permutation π. The goal of the routing protocol is to ensure that all k communications proceed simultaneously without blocking. Owing to the recursive construction of the quantum Beneš network and the realizability of non-blocking 2×2 quantum switches, the routing protocol only needs to guarantee the absence of blocking between the input and switching layers, as well as between the switching and output layers.

We first present the routing protocol for quantum Beneš networks of size $k = 2^n$. The modifications required for arbitrary k, particularly when an odd-sized network is decomposed into subnetworks of unequal sizes, are described at the end of this subsection. The procedure is as follows:

1. Construct a graph with k vertices, labeled from 1 to k. For the ith vertex, the index of its target output is denoted by $\pi(i)$.
2. Add an edge between any two vertices whose indices differ by $k/2$.
3. Similarly, add an edge between any two vertices whose target indices differ by $k/2$.
4. Partition the graph into its connected components. In each component, mark the vertex with the largest index yellow and then alternately mark adjacent vertices red and yellow until all vertices are colored.
5. Route the source nodes represented by yellow vertices through the upper subnetwork and those represented by red vertices through the lower subnetwork.

By following the above steps, entanglement can be simultaneously generated between multiple source-destination pairs.

The correctness of this protocol can be rigorously established using mathematical induction. For $k = 2$, the network reduces to a fully connected structure of size 2, for which the desired mapping can be achieved straightforwardly. We then show that if the quantum Beneš network of size k functions correctly, the network of size $2k$ also functions correctly. As mentioned above, the quantum Beneš network of size $2k$ can be divided into three layers: the input layer, the switching layer, and the output layer. The switching layer contains two quantum Beneš subnetworks of size k, referred to as the upper subnetwork and the lower subnetwork. The input layer routes the $2k$ source nodes to either the upper or the lower subnetwork, ensuring that no two source nodes arrive at the same repeater. The output layer routes nodes from the switching layer to their designated destination nodes. To satisfy these constraints, all source nodes must be partitioned into two disjoint sets: one routed to the upper subnetwork and the other to the lower subnetwork. To avoid collisions at the nodes, the following conditions must be enforced:

1. The ith source node ($i \leq k$) and the $(i + k)$th source node must be routed through different subnetworks.
2. Any two source nodes whose destination indices differ by k must also be routed through different subnetworks.

To model these constraints, we construct an edge-labeled multigraph, referred to as the topology graph, in which each vertex represents a source node and each edge requires its two endpoints to be routed through different subnetworks. An input-constraint edge connects the ith and $(i + k)$th source nodes, whereas a target-constraint edge connects two source nodes whose destination indices differ by k. The input-constraint edges form a perfect matching on the $2k$ vertices. Because π is a permutation, the target-constraint edges also form a perfect matching. Consequently, every vertex is incident to exactly one edge of each type.

The union of the two perfect matchings decomposes into vertex-disjoint cycles in which input-constraint and target-constraint edges alternate. If the two types of constraint edges connect the same pair of vertices, they are retained as two labeled parallel edges and form a cycle of length 2. Every connected component is therefore an even-length cycle and admits a proper two-coloring.

The two-coloring is not unique unless an additional convention is imposed. Each connected component has two possible colorings that differ only by an interchange of the two colors. Thus, if the topology graph has c connected components, it admits 2^c proper two-colorings when the color labels are distinguished. In our protocol, the vertex with the largest index in each component is assigned yellow. The colors of the remaining vertices are then uniquely determined by alternating around the cycle. The coloring produced by the protocol is therefore unique under this convention.

Yellow and red vertices are routed through the upper and lower subnetworks, respectively. Because the endpoints of every input-constraint and target-constraint edge have different colors, each subnetwork receives exactly k source nodes with k distinct target outputs. By the induction hypothesis, the assigned permutation can be realized within each size-k quantum Beneš subnetwork. Moreover, no repeater in the input or output layer is traversed by more than one path. Because every repeater within each size-k subnetwork performs at most one BSM, every repeater in the resulting size-$2k$ network also performs at most one BSM. All $2k$ source-destination pairs can therefore establish entanglement simultaneously without blocking.

At any recursive step with an even network size, the source nodes are partitioned equally between the two subnetworks using the procedure described above. For an odd size k, the same graph-coloring principle is used, but the upper and lower subnetworks contain $\lfloor k/2 \rfloor$ and $\lceil k/2 \rceil$ input-output pairs, respectively. The kth input and output nodes are

connected exclusively to the larger lower subnetwork. Accordingly, no constraint edge is added for the kth source node or for the source node whose target is D_k. The resulting topology graph consists of disjoint even cycles together with either an isolated vertex or a chain whose endpoints correspond to these restricted nodes. The isolated vertex, or the appropriate endpoint of the chain, is assigned to the lower subnetwork, and the remaining vertices along the chain are colored alternately. The even-cycle components are colored as in the power-of-2 case. The two subnetworks consequently receive at most $\lfloor k/2 \rfloor$ and $\lceil k/2 \rceil$ source-destination pairs, respectively, and recursive application of the protocol realizes an arbitrary permutation for any positive integer k. Further details and a complete proof are provided in the Supplementary Material.

The rearrangeably non-blocking property established above guarantees the existence of non-conflicting paths under ideal resource availability; it does not guarantee the success of the probabilistic physical operations along those paths.

3.3.A quantum Beneš network of size 4. Here, we illustrate a quantum Beneš network of size 4 as an example. There are 4 source nodes $\{S_1, S_2, S_3, S_4\}$ and 4 destination nodes $\{D_1, D_2, D_3, D_4\}$ in this network. Let π be any permutation of the set $\{1, 2, 3, 4\}$, and let $D_{\pi(i)}$ denote the destination node corresponding to source node S_i. To simultaneously generate entanglement between all pairs $(S_i, D_{\pi(i)})$, the paths must be arranged such that no repeater is required to perform two BSMs. In other words, the paths connecting nodes S_i and $D_{\pi(i)}$ cannot pass through the same repeater. As shown in Fig. 4, the quantum Beneš network of size 4 consists of four levels and can be conceptually divided into three layers. The first layer is the input layer, comprising level 1. It connects the source nodes to the network and routes them to either the upper or the lower subnetwork. The second layer is the switching layer, comprising levels 2 and 3. This layer can be further divided into two quantum Beneš subnetworks of size 2, referred to as the upper subnetwork and the lower subnetwork. The last layer is the output layer, comprising level 4, which connects the destination nodes to

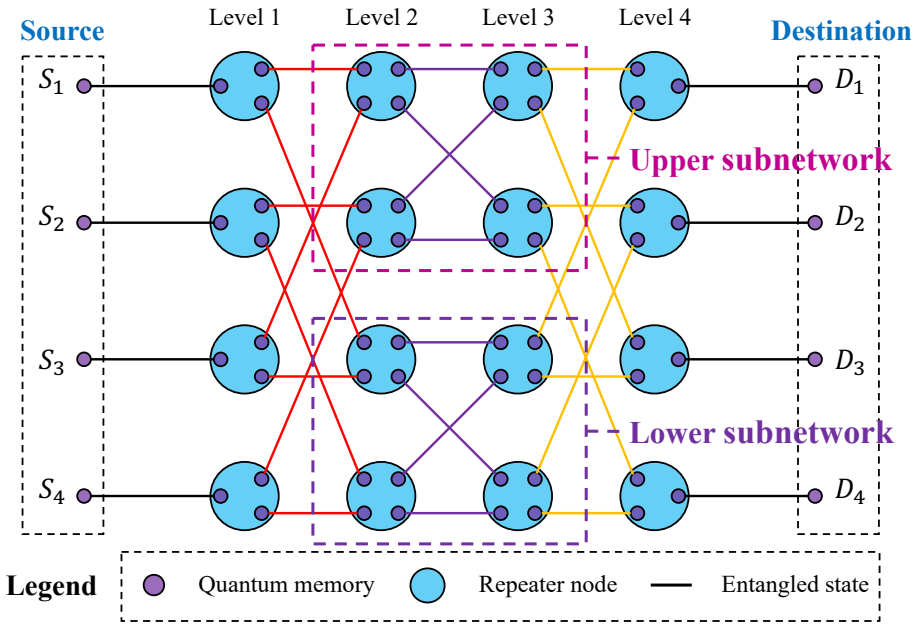


Figure 4: A quantum Beneš network of size 4, comprising four levels: Level 1 (input layer) connects the source nodes to the subnetwork; Levels 2 and 3 form the switching layer and consist of two subnetworks; Level 4 (output layer) connects the destination nodes to the subnetwork. The repeater and quantum memory symbols follow the definitions in Fig. 1. The Bell pairs connecting the external source and destination nodes to the switching fabric are included for illustration and are excluded from the resource count in Sec. 3.4.

the subnetwork. Each repeater in the input or output layer shares entangled states with two repeaters in the switching layer.

Figure 5(a) illustrates a specific routing task in the quantum Beneš network of size 4. The objective is to simultaneously establish entanglement between the pairs $\{S_1, D_3\}$, $\{S_2, D_1\}$, $\{S_3, D_4\}$, and $\{S_4, D_2\}$. Following the procedure described above, one can construct the corresponding topology graph shown in Fig. 5(b) and label its vertices as either yellow or red. Edges are plotted in two colors: blue solid edges represent output constraints, while purple dashed edges represent input constraints. Vertices marked yellow (vertices 1 and 4) establish entanglement with target vertices via the upper subnetwork, while vertices marked red (vertices 2 and 3) use the lower subnetwork. Once it is determined whether a connection is established via the upper or lower subnetwork, the paths between the input and output layers become uniquely defined.

3.4.Resource and performance comparison. The entanglement cost of a quantum Beneš network can be derived

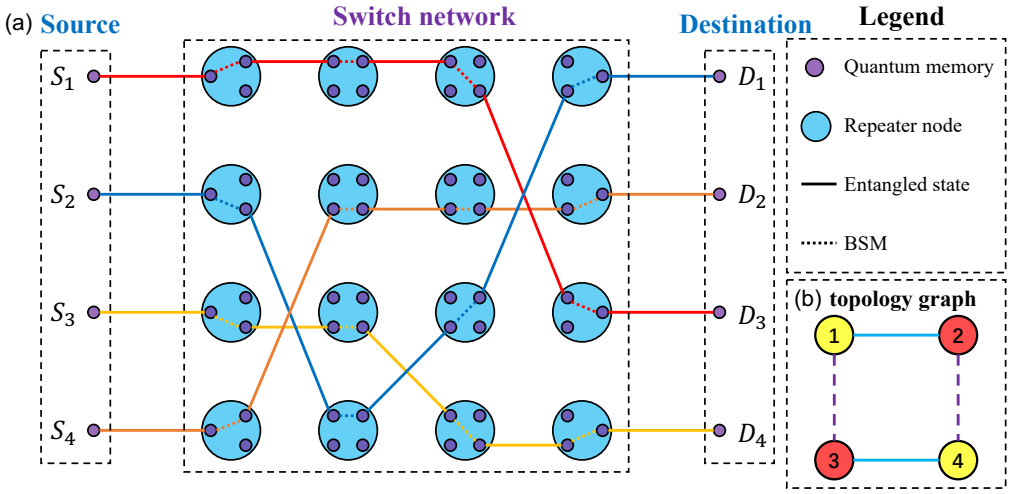


Figure 5: A specific routing task for a quantum Beneš network of size 4. (a) The network diagram and the corresponding routing configuration. The solid lines represent shared entangled states, whereas the dashed lines denote BSMs. Distinct colors indicate different end-to-end entanglement paths. The repeater and quantum memory symbols follow the definitions in Fig. 1. (b) The corresponding topology graph constructed from the input and target constraints and used to assign the source nodes to the upper and lower subnetworks.

recursively. For $k = 2^n$, a network of size k consists of two subnetworks of size $k/2$ and $4k$ additional Bell pairs connecting the input and output layers to the subnetworks. Starting from the size-2 network with four Bell pairs gives a total resource count of $(4\log_2 k - 2)k$. Here, the count refers to the standard switching fabric and excludes optional Bell pairs connecting external terminals to its input and output ports. Thus, the 4×4 switching fabric requires 24 Bell pairs, whereas Fig. 4 additionally includes $2k = 8$ access Bell pairs for illustration. For arbitrary k, the resource requirement is upper-bounded by that of a network of size $2^{\lceil \log_2 k \rceil}$ and therefore scales as $\mathcal{O}(k \log k)$.

In practice, candidate links may attempt heralded entanglement generation independently and in parallel and report their availability to a central controller. Switching can begin once the available links support one complete set of non-conflicting paths; it is unnecessary to wait for every candidate link in the fabric. As k increases, the logarithmic growth of the route depth increases the number of link-level Bell pairs required along each route and generally increases the preparation time. The actual preparation time also depends on the link-generation probability and attempt duration, the available alternative routing configurations, and the link-state-dependent routing strategy.

Quantum memory imperfections introduce an additional trade-off. Stored Bell pairs lose fidelity through decoherence and may be discarded after a prescribed storage-time cutoff, after which entanglement generation is restarted on the corresponding links. Entanglement purification may also be applied at the link layer before a pair is made available to the routing protocol. These measures can improve the retained fidelity but increase the preparation time and the consumption of raw Bell pairs, memory qubits, and classical communication. Their optimization requires a platform-specific model and is left for future work.

For a full k-pair task, each participating switching node performs one BSM for one source-destination path. A failed BSM or a faulty switching node prevents the connection passing through that node from being established, although connections along unaffected paths may still succeed. The complete k-pair task therefore fails in that attempt. A probabilistic BSM failure is transient, but the Bell pairs consumed by the affected swapping operations must be regenerated before another attempt. By contrast, a faulty switching node remains unavailable. Because all switching nodes in each layer are required to support the k simultaneous connections, the original Beneš fabric cannot recover from such a node failure through rerouting alone; repair, replacement, or additional redundant switching resources are required.

With finite BSM success probability, rearrangeable non-blocking remains a topological property: non-conflicting paths still exist for every permutation, but their physical establishment becomes probabilistic. The BSM success probability can be improved using ancillary-photon-assisted linear-optical schemes that exceed the conventional 50% limit [75], or through loss-tolerant tree-graph-state encodings and indirect measurements that enable near-deterministic logical BSMs [76,77]. These approaches require additional photonic, detection, and memory resources, and their integration into the present architecture is left for future work.

To quantitatively characterize the proposed architecture, we compare it with direct input-output entanglement and the quantum crossbar protocol in Ref. [52]. The comparison considers the ideal establishment of end-to-end entanglement for a k-pair permutation. A classical communication round refers to one parallel feed-forward round in which BSM outcomes are transmitted to the destination nodes; entanglement-generation heralding and routing computation are excluded. Network depth denotes the number of intermediate processing stages along an input-output route.

Direct entanglement requires k^2 Bell pairs but no intermediate BSM and has constant network depth. The quantum Beneš network contains $2\log_2 k$ repeater layers, with all k repeaters in each layer performing one BSM for a full permutation, giving $2k\log_2 k$ BSMs in total. In the quantum crossbar protocol, Bell-pair generation and BSMs alternate along the selected routes. Although its architectural Bell-pair resource scales as $\mathcal{O}(k^2)$, its task-specific Bell-pair consumption, BSM count, and classical communication rounds depend on the permutation, route lengths, and feasible assignment of the even and odd distribution schemes. These quantities are denoted by permutation-dependent (PD) in Table 1.

Table 1: Comparison of Bell-pair-based schemes for a k-pair input-output permutation under ideal operations. The classical communication rounds exclude entanglement-generation heralding and routing computation. PD denotes permutation-dependent.

Scheme	Direct entanglement	Quantum crossbar network [52]	Quantum Beneš network
Bell-pair resource scaling	$\mathcal{O}(k^2)$	$\mathcal{O}(k^2)$	$\mathcal{O}(k\log k)$
Number of BSMs	0	PD	$2k\log_2 k$
Classical communication rounds	0	PD	1
Network depth	$\mathcal{O}(1)$	$\mathcal{O}(k)$	$\mathcal{O}(\log k)$
Rearrangeably non-blocking for arbitrary permutations	Yes	Not guaranteed for $k \geq 4$	Yes

Table 2: Bell-pair counts and network depths for representative network sizes. Task-specific quantum crossbar consumption is not listed because it is permutation-dependent.

Quantity	$k=4$	$k=8$	$k=16$	$k=32$	$k=256$	$k=1024$
Direct entanglement: Bell pairs	16	64	256	1024	65536	1048576
Quantum Beneš: Bell pairs	24	80	224	576	7680	38912
Quantum Beneš: network depth	4	6	8	10	16	20

Tables 1 and 2 show that direct entanglement provides constant network depth but has quadratic Bell-pair scaling. The quantum Beneš network requires more Bell pairs for $k = 4$ and 8, whereas its resource advantage appears at $k = 16$ and increases with network size. For example, at $k = 256$ and 1024, the Bell-pair requirement is reduced from 65536 to 7680 and from 1048576 to 38912, respectively, corresponding to reductions of approximately 88.3% and 96.3%, while the associated network depths remain 16 and 20. It therefore provides a scalable trade-off rather than minimizing both resources and depth at every finite size: the Bell-pair scaling is reduced to $\mathcal{O}(k\log k)$ while logarithmic network depth and rearrangeably non-blocking routing are retained.

For the quantum crossbar protocol, task-specific resource consumption cannot be expressed uniquely as a function of k. Moreover, classical crossbar non-blocking does not guarantee non-blocking entanglement distribution when each intermediate node is restricted to one BSM per operational cycle. Ref. [52] identifies permutations that cannot be completed within one cycle under this restriction for $k \geq 4$.

QNC and MQNC are not included in the tables because they generally address prescribed topologies and traffic patterns rather than universal k-pair permutation switching [50,51,54,55]. Their resources and operation counts therefore depend on the particular topology and communication task. Previous work on a butterfly network found repeater-based QNC to be more sensitive to local-operation errors than the corresponding entanglement-swapping scheme [54]. This observation is qualitatively relevant because the present Beneš network is also based on entanglement swapping, although a quantitative comparison would require a common topology, communication task, and physical noise model. Clos-type switching fabrics based on multipartite graph states have also been proposed [78], but their graph-state-qubit resources are not included in the present Bell-pair-based benchmark.

Finally, network depth should be distinguished from measurement-operation depth. Although the quantum Beneš network has $\mathcal{O}(\log k)$ repeater layers, the BSMs at different nodes are independent and can be performed simultaneously.

Their outcomes are transmitted to the destinations in one classical feed-forward round, where the corresponding local corrections are applied. This process can be regarded as multihop teleportation with simultaneous measurements [64]; under the ideal assumptions adopted here, its measurement-operation depth is independent of the number of repeater layers.

4.Conclusion. This work develops a quantum network architecture based on the Beneš switching topology that achieves resource-efficient, non-blocking, and low-latency performance. By adapting the hierarchical routing principle from classical telecommunications, the framework establishes $\mathcal{O}(k \log k)$ resource scaling for full k-processor connectivity. The resource-efficiency advantage is platform-independent and applies universally to quantum systems capable of local operations and entanglement swapping. The framework enables concurrent multi-pair entanglement distribution, dynamic resource routing, and scalable connectivity among arbitrary numbers of quantum processors. Photonic systems possess practical advantages for implementing this architecture: mature photonic switching components, feasible integrated-circuit implementation, and compatibility with existing telecommunications infrastructure provide a potential route toward experimental implementation. The routing protocol specifies an appropriate measurement scheme for each node, thereby enabling non-blocking communication. Moreover, the simultaneous and independent measurement strategy reduces end-to-end communication delay, giving the network an inherent low-latency advantage.

Several avenues naturally emerge from this work. An immediate priority is to assess the robustness of resource-efficient Beneš networks under realistic noise models and decoherence channels across different quantum platforms, in order to refine performance predictions and identify concrete optimization opportunities. In parallel, there is scope to develop more sophisticated quantum routing protocols that adapt dynamically to network conditions and computational workloads, potentially improving both entanglement utilization and overall throughput. A further direction is to explore how such architectures can be interfaced with quantum error correction, where suitable integration strategies may offer complementary benefits in terms of fault tolerance and effective resource cost. On the implementation side, photonic platforms call for detailed technical studies of photon-loss mitigation, efficient wavelength conversion, low-loss integrated fabrication, and scalable multi-stage switching elements, which together will determine realistic experimental requirements. In addition, hybrid schemes that combine photonic entanglement distribution with matter-based quantum processors may reveal useful trade-offs among coherence time, connectivity, and implementation complexity. Taken together, these directions build upon the theoretical framework established here, which identifies the key architectural principles and performance boundaries of quantum Beneš networks, and positions this class of resource-efficient, Beneš-inspired switching architectures as a promising route toward practically scalable distributed quantum information processing.

Acknowledgements. We thank Jian-Long Liu, Jun Li, and Xiao-Hui Bao for very insightful discussions and valuable suggestions. This work has been supported by the National Natural Science Foundation of China (Grants No. 62375252, 11874346 and 12174375), the National Key R&D Program of China (Grants No. 2019YFA0308700), the Anhui Initiative in Quantum Information Technologies (Grants No. AHY060200), and the Quantum Science and Technology-National Science and Technology Major Project (Grant No. 2021ZD0301100 and No. 2021ZD0301400).

References

[1] Kimble H J 2008 *Nature* **453** 1023

[2] Wehner S, Elkouss D and Hanson R 2018 *Science* **362** eaam9288

[3] Awschalom D, Berggren K K, Bernien H, Bhave S, Carr L D, Davids P, Economou S E, Englund D, Faraon A, Fejer M, Guha S, Gustafsson M V, Hu E, Jiang L, Kim J, Korzh B, Kumar P, Kwiat P G, Lončar M, Lukin M D, Miller D A, Monroe C, Nam S W, Narang P, Orcutt J S, Raymer M G, Safavi-Naeini A H, Spiropulu M, Srinivasan K, Sun S, Vučković J, Waks E, Walsworth R, Weiner A M and Zhang Z 2021 *PRX Quantum* **2** 017002

[4] Briegel H J, Dür W, Cirac J I and Zoller P 1998 *Phys. Rev. Lett.* **81** 5932

[5] Gisin N and Thew R 2007 *Nat. Photonics* **1** 165

[6] Barral D, Cardama F J, Díaz-Camacho G, Faílde D, Llovo I F, Mussa-Juane M, Vázquez-Pérez J, Villasuso J, Piñeiro C, Costas N, Pichel J C, Pena T F and Gómez A 2025 *Comput. Sci. Rev.* **57** 100747

[7] Caleffi M, Amoretti M, Ferrari D, Illiano J, Manzalini A and Cacciapuoti A S 2024 *Comput. Netw.* **254** 110672

[8] Ekert A K 1991 *Phys. Rev. Lett.* **67** 661

[9] Wang M H, Xiang Y, Kang H J, Han D M, Liu Y, He Q Y, Gong Q H, Su X L and Peng K C 2020 *Phys. Rev. Lett.* **125** 260506

[10] Luo M X 2022 *Phys. Rev. Res.* **4** 013203

[11] Xu F H, Ma X F, Zhang Q, Lo H K and Pan J W 2020 *Rev. Mod. Phys.* **92** 025002

[12] Duan L M and Monroe C 2010 *Rev. Mod. Phys.* **82** 1209

[13] Bernien H, Hensen B, Pfaff W, Koolstra G, Blok M S, Robledo L, Taminiau T H, Markham M, Twitchen D J, Childress L and Hanson R 2013 *Nature* **497** 86

[14] Bennett C H, Brassard G, Crépeau C, Jozsa R, Peres A and Wootters W K 1993 *Phys. Rev. Lett.* **70** 1895

[15] Van Meter R and Devitt S J 2016 *Computer* **49** 31

[16] Cuomo D, Caleffi M and Cacciapuoti A S 2020 *IET Quantum Commun.* **1** 3

[17] Marcikic I, de Riedmatten H, Tittel W, Zbinden H, Legré M and Gisin N 2004 *Phys. Rev. Lett.* **93** 180502

[18] Liu J L, Luo X Y, Yu Y, Wang C Y, Wang B, Hu Y, Li J, Zheng M Y, Yao B, Yan Z, Teng D, Jiang J W, Liu X B, Xie X P, Zhang J, Mao Q H, Jiang X, Zhang Q, Bao X H and Pan J W 2024 *Nature* **629** 579

[19] Kucera S, Haen C, Arenskötter E, Bauer T, Meiers J, Schäfer M, Boland R, Yahyapour M, Lessing M, Holzwarth R, Becher C and Eschner J 2024 *npj Quantum Inf.* **10** 88

[20] Yin J, Cao Y, Li Y H, Liao S K, Zhang L, Ren J G, Cai W Q, Liu W Y, Li B, Dai H, Li G B, Lu Q M, Gong Y H, Xu Y, Li S L, Li F Z, Yin Y Y, Jiang Z Q, Li M, Jia J J, Ren G, He D, Zhou Y L, Zhang X X, Wang N, Chang X, Zhu Z C, Liu N L, Chen Y A, Lu C Y, Shu R, Peng C Z, Wang J Y and Pan J W 2017 *Science* **356** 1140

[21] Ren J G, Xu P, Yong H L, Zhang L, Liao S K, Yin J, Liu W Y, Cai W Q, Yang M, Li L, Yang K X, Han X, Yao Y Q, Li J, Wu H Y, Wan S, Liu L, Liu D Q, Kuang Y W, He Z P, Shang P, Guo C, Zheng R H, Tian K, Zhu Z C, Liu N L, Lu C Y, Shu R, Chen Y A, Peng C Z, Wang J Y and Pan J W 2017 *Nature* **549** 70

[22] de Riedmatten H, Marcikic I, van Houwelingen J A W, Tittel W, Zbinden H and Gisin N 2005 *Phys. Rev. A* **71** 050302

[23] Chen Y A, Zhang Q, Chen T Y, Cai W Q, Liao S K, Zhang J, Chen K, Yin J, Ren J G, Chen Z, Han S L, Yu Q, Liang K, Zhou F, Yuan X, Zhao M S, Wang T Y, Jiang X, Zhang L, Liu W Y, Li Y, Shen Q, Cao Y, Lu C Y, Shu R, Wang J Y, Li L, Liu N L, Xu F H, Wang X B, Peng C Z and Pan J W 2021 *Nature* **589** 214

[24] Sun Q C, Mao Y L, Jiang Y F, Zhao Q, Chen S J, Zhang W, Zhang W J, Jiang X, Chen T Y, You L X, Li L, Huang Y D, Chen X F, Wang Z, Ma X F, Zhang Q and Pan J W 2017 *Phys. Rev. A* **95** 032306

[25] Craddock A N, Lazenby A, Portmann G B, Sekelsky R, Flament M and Namazi M 2024 *PRX Quantum* **5** 030330

[26] Thomas J M, Yeh F I, Chen J H, Mambretti J J, Kohlert S J, Kanter G S and Kumar P 2024 *Optica* **11** 1700

[27] Zhuang S C, Li B, Zheng M Y, Zeng Y X, Wu H N, Li G B, Yao Q, Xie X P, Li Y H, Qin H, You L X, Xu F, Yin J, Cao Y, Zhang Q, Peng C Z and Pan J W 2025 *Phys. Rev. Lett.* **134** 230801

[28] Xie Y, Hao Y, Lin Y, Sun Y, Wang D, Guo C, Chen N, Liu Y and Tang J 2025 *Opt. Express* **33** 46545

[29] Huang J, Han H, Li J, Li J, Peng T, Yu W, Wu C, Sun S and Liu B 2026 *Sci. China Phys. Mech. Astron.* **69** 220315

[30] Zhong H, Hu Q, Zuo Z, Mao Y, Huang D and Guo Y 2026 *Opt. Express* **34** 17370

[31] Kielpinski D, Monroe C and Wineland D J 2002 *Nature* **417** 709

[32] Akhtar M, Bonus F, Lebrun-Gallagher F R, Johnson N I, Siegele-Brown M, Hong S, Hile S J, Kulmiya S A, Weidt S and Hensinger W K 2023 *Nat. Commun.* **14** 531

[33] Wan Y, Kienzler D, Erickson S D, Mayer K H, Tan T R, Wu J J, Vasconcelos H M, Glancy S, Knill E, Wineland D J, Wilson A C and Leibfried D 2019 *Science* **364** 875

[34] Humphreys P C, Kalb N, Morits J P J, Schouten R N, Vermeulen R F L, Twitchen D J, Markham M and Hanson R 2018 *Nature* **558** 268

[35] Knaut C M, Suleymanzade A, Wei Y C, Assumpcao D R, Stas P J, Huan Y Q, Machielse B, Knall E N, Sutula M, Baranes G, Sinclair N, De-Eknamkul C, Levonian D S, Bhaskar M K, Park H, Lončar M and Lukin M D 2024 *Nature* **629** 573

[36] van Leent T, Bock M, Fertig F, Garthoff R, Eppelt S, Zhou Y, Malik P, Seubert M, Bauer T, Rosenfeld W, Zhang W, Becher C and Weinfurter H 2022 *Nature* **607** 69

[37] Daiss S, Langenfeld S, Welte S, Distante E, Thomas P, Hartung L, Morin O and Rempe G 2021 *Science* **371** 614

[38] Main D, Drmota P, Nadlinger D P, Ainley E M, Agrawal A, Nichol B C, Srinivas R, Araneda G and Lucas D M 2025 *Nature* **638** 383

[39] Wang J, Sciarrino F, Laing A and Thompson M G 2020 *Nat. Photonics* **14** 273

[40] Munro W J, Azuma K, Tamaki K and Nemoto K 2015 *IEEE J. Sel. Top. Quantum Electron.* **21** 78

[41] Azuma K, Economou S E, Elkouss D, Hilaire P, Jiang L, Lo H K and Tzitrin I 2023 *Rev. Mod. Phys.* **95** 045006

[42] Cirac J I, Ekert A K, Huelga S F and Macchiavello C 1999 *Phys. Rev. A* **59** 4249

[43] Cacciapuoti A S, Caleffi M, Tafuri F, Cataliotti F S, Gherardini S and Bianchi G 2020 *IEEE Netw.* **34** 137

[44] Lu H, Li Z D, Yin X F, Zhang R, Fang X X, Li L, Liu N L, Xu F H, Chen Y A and Pan J W 2019 *npj Quantum Inf.* **5** 89

[45] Hahn F, Pappa A and Eisert J 2019 *npj Quantum Inf.* **5** 76

[46] Pant M, Krovi H, Towsley D, Tassiulas L, Jiang L, Basu P, Englund D and Guha S 2019 *npj Quantum Inf.* **5** 25

[47] Shi Y and Soljanin E 2006 *Proceedings of the 40th Annual Conference on Information Sciences and Systems, March 22–24, 2006, Princeton, NJ, USA* p. 871

[48] Hayashi M, Iwama K, Nishimura H, Raymond R and Yamashita S 2007 *STACS 2007* ed Thomas W and Weil P (Berlin, Heidelberg: Springer Berlin Heidelberg) p. 610

[49] Hayashi M 2007 *Phys. Rev. A* **76** 040301

[50] Satoh T, Le Gall F and Imai H 2012 *Phys. Rev. A* **86** 032331

[51] Epping M, Kampermann H and Bruß D 2016 *New J. Phys.* **18** 103052

[52] Ciobanu B C, Verzotti L P and Popescu P G 2024 *Sci. Rep.* **14** 11714

[53] Ahlswede R, Cai N, Li S Y and Yeung R 2000 *IEEE Trans. Inf. Theory* **46** 1204

[54] Satoh T, Ishizaki K, Nagayama S and Van Meter R 2016 *Phys. Rev. A* **93** 032302

[55] Matsuo T, Satoh T, Nagayama S and Van Meter R 2018 *Phys. Rev. A* **97** 062328

[56] Akibue S and Murao M 2016 *IEEE Trans. Inf. Theory* **62** 6620

[57] Clos C 1953 *Bell Syst. Tech. J.* **32** 406

[58] Feng T Y 1981 *Computer* **14** 12

[59] Duato J, Yalamanchili S and Ni L M 2002 *Interconnection Networks: An Engineering Approach* 1st ed (San Francisco: Morgan Kaufmann)

[60] Dally W J and Towles B 2004 *Principles and Practices of Interconnection Networks* (Morgan Kaufmann)

[61] Beneš V E 1964 *Bell Syst. Tech. J.* **43** 1619

[62] Chang C and Melhem R 1997 *Parallel Process. Lett.* **7** 279

[63] Jumandi Z, Samsudin A and Budiarto R 2004 *Proceedings of the International Conference on Information and Communication Technologies: From Theory to Applications, April 19–23, 2004, Damascus, Syria* p. 665

[64] Wang K, Yu X T, Lu S L and Gong Y X 2014 *Phys. Rev. A* **89** 022329

[65] Pan J W, Bouwmeester D, Weinfurter H and Zeilinger A 1998 *Phys. Rev. Lett.* **80** 3891

[66] Leung D, Oppenheim J and Winter A 2010 *IEEE Trans. Inf. Theory* **56** 3478

[67] Pan X B, Xu G, Li Z P, Chen X B and Yang Y X 2021 *Quantum Inf. Process.* **20** 65

[68] Nguyen H V, Babar Z, Alanis D, Botsinis P, Chandra D, Mohd Izhar M A, Ng S X and Hanzo L 2017 *IEEE Access* **5** 17288

[69] Kobayashi H, Le Gall F, Nishimura H and Rötteler M 2009 *Automata, Languages and Programming* ed Albers S, Marchetti-Spaccamela A, Matias Y, Nikoletseas S and Thomas W (Berlin, Heidelberg: Springer Berlin Heidelberg) p. 622

[70] Kobayashi H, Le Gall F, Nishimura H and Rötteler M 2011 *Proceedings of the IEEE International Symposium on Information Theory, July 31–August 5, 2011, St. Petersburg, Russia* p. 109

[71] Pathumsoot P, Matsuo T, Satoh T, Hajdušek M, Suwanna S and Van Meter R 2020 *Phys. Rev. A* **101** 052301

[72] Spanke R A and Beneš V E 1987 *Appl. Opt.* **26** 1226

[73] Ratan R, Shukla M K and Oruc A Y 2007 *Proceedings of the 41st Annual Conference on Information Sciences and Systems, March 14–16, 2007, Baltimore, MD, USA* p. 789

[74] Rall H and Tame M 2024 *Phys. Rev. A* **110** 022602

[75] Bayerbach M J, D'Aurelio S E, van Loock P and Barz S 2023 *Sci. Adv.* **9** eadf4080

[76] Varnava M, Browne D E and Rudolph T 2006 *Phys. Rev. Lett.* **97** 120501

[77] Hilaire P, Barnes E, Economou S E and Grosshans F 2021 *Phys. Rev. A* **104** 052623

[78] Illiano J, De Risi C, Cacciapuoti A S and Caleffi M 2026 arXiv: 2606.17773 [quant-ph]